Injection locking in self-oscillating magnetometers

Alexander P. Nikitin and Nigel G. Stocks

Injection locking (IL) is a well-known phenomenon that occurs in nonlinear oscillators subject to external periodic or non-periodic signals. It is a phenomenon of induced synchronization that occurs when an external (injection) signal locks the frequency of the oscillator to the frequency of the external signal. This form of synchronisation is relatively straightforward to implement because it does not require specially organised feedback as is the case with phase locked loop. Circuits that exploit IL can have very simple designs and be applied to a broad range of applications such as to synchronize frames and lines in early television sets, to synchronize lasers, to function as a. c. voltmeters, field-intensity meters, amplifier-limiters and AM and FM detectors. However, the focus of this article is the recent application of IL to magnetic field sensors. This novel application highlights the potential benefits of the IL approach but also some of the complexities and opportunities for further development. As with all measurement systems, the consideration of noise is paramount in the design of magnetic sensors. Noise reduction and mitigation strategies are essential. IL can be employed as a noise mitigations strategy in magnetometers that utilise self-oscillations as part of their detection paradigm; it can stabilize the oscillation frequency, potentially simplifying the measurement circuitry, and in some circumstances improve the signal-to-noise ratio. Here we review some magnetometers that have successfully exploited IL principles and highlight design options. We also propose a new circuit that is simple to implement and more straightforward to analyse.

Synchronization

IL is a synchronization phenomenon. Following many other texts [1, 2, 3, 4] we introduce synchronization by means of the Van der Pol (VdP) oscillator driven by a periodic signal.

The Van der Pol oscillator Fig. 1(a) is a standard LC-resonance circuit with a negative resistor $\bar{R}$ that compensates for the energy loss. The equation for the current is well known [2, 3, 5],

$$\ddot{x} - \varepsilon(1 - \alpha x^2)\dot{x} + \omega_0^2 x = \omega^2 B\cos(\omega t), \quad (1)$$

where x is the current, ω_0 is the natural frequency of the oscillator, ϵ and α are parameters, and B and ω are the amplitude and frequency of the locking signal respectively. If the resonance circuit has a high Q

(i.e. $\varepsilon \ll 1$), the synchronized oscillations of the current have an almost cosine form, $A\cos(\omega t + \varphi)$, where A is the amplitude of oscillations and φ is the phase. For high Q systems A and φ are almost constant during one period of oscillation, this enables simplified equations for the amplitude and phase to be obtained, [2, 3, 4],

$$\dot{A} = \frac{\varepsilon}{2}\left(1 - \frac{A^2}{A_0^2}\right) A - \frac{\omega_0 B}{2}\sin\varphi, \qquad (2)$$

$$\dot{\varphi} = \Delta - \frac{\omega_0 B}{2A}\cos\varphi, \qquad (3)$$

where $\Delta = (\omega_0 - \omega)$ ($\Delta \ll \omega$) is the frequency detuning, and $A_0 = 2\sqrt{\alpha}$ is the amplitude of the non-synchronized oscillations.

When the system is synchronized the amplitude A and the phase φ are stable, so $\dot{A} = 0$ and $\dot{\varphi} = 0$ and hence Eqs. (2) and (3) transformed into algebraic equations whose solutions we denote A_{st} and φ_{st}. It is easy to show that for small B, $A_{st} \simeq A_0$ and φ takes on discrete values $\varphi_{st} \simeq \arccos\left(\frac{2A_0\Delta}{\omega_0 B}\right) + 2\pi n$, where n is an integer. In addition, we can find boundaries of the synchronization region in the parameter space B and Δ (the Arnold tongue [4]): $\Delta = \frac{\omega_0 B}{2A_0}$ for $\Delta > 0$, and $\Delta = -\frac{\omega_0 B}{2A_0}$ for $\Delta < 0$.

Synchronization is illustrated in Fig. 1(b,c). Plotted is the oscillator current $x(t)$ against the periodic locking signal $S(t) = B\cos(\omega t)$ for the unlocked (Fig. 1(b)) and locked cases (Fig. 1(c)).

To take into account the impact of noise the above analysis has to be modified slightly. The affect of noise on the amplitude of the oscillations is modest: A fluctuates near its stable value A_{st} [5] and only weakly depends on parameters B and ω, hence these fluctuations will be neglected in the remaining discussion. However noise can have a more significant impact on the phase. To understand

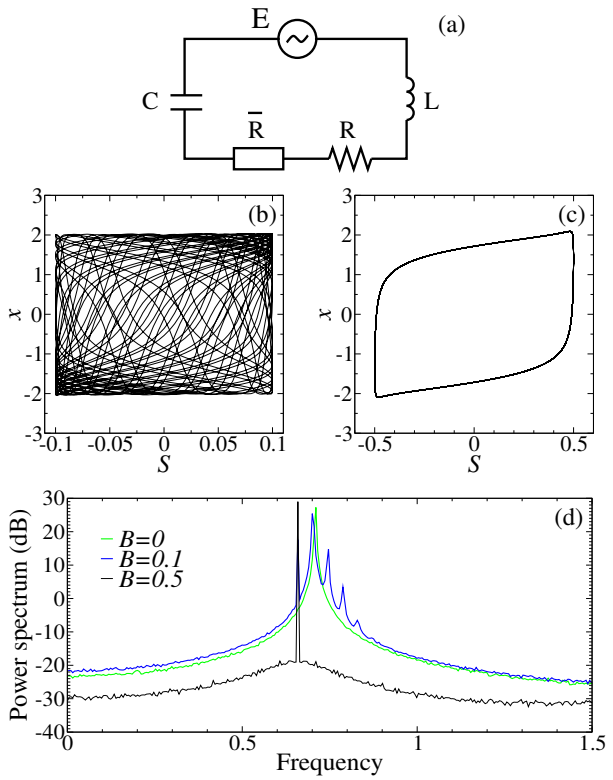

Figure 1: (a) The Van der Pol oscillator circuit; (b,c) Lissajous figures: plot of circuit oscillations, $x(t)$, versus periodic locking signal, $S(t) = B\cos(\omega t)$, for (b) unlocked and (c) locked oscillations; (d) power spectra for different values of the locking signal amplitude. Parameters are $\epsilon = 3$, $\omega_0 = 1$, $\omega = 0.658$, $\alpha = 1$ and the noise intensity $D_n = 0.001$ of Gaussian white noise that is added to Eq. (1).

why we re-write Eq. (3) as,

$$\dot{\varphi} = -\frac{dU(\varphi)}{d\varphi} + \xi(t), \quad U(\varphi) = \varphi\Delta - \frac{\omega_0 B}{2A}\sin\varphi, \tag{4}$$

where $\xi(t)$ represents the noise in the system [5]. These equations can be interpreted as a Brownian particle diffusing in a tilted (for $\Delta \neq 0$) periodic potential $U(\varphi)$ with potential minima located at the values φ_{st}. Noise can induce two different types of dynamics: small fluctuations about the potential minima and large fluctuations caused by jumps from one potential minima to another, so called phase jumps. Each jump causes a change of phase of $\pm 2\pi$, the sign indicates whether the jump is to the left (-ve) or the right (+ve). Random phase jumps manifest as momentary 'slips' in synchronization and result in strong phase diffusion [5].

A strategy for reducing phase diffusion is to reduce the probability of phase jumps. A simple analysis of Eq. (4) reveals that the barrier heights between the potential minima are proportional to B. Thus increasing B can significantly reduce phase diffusion by increasing the barrier heights. For non-zero detuning Δ the barrier height, Δ_l, for a jump to the left is different to the barrier height, Δ_r, for a right jump to the right. The rate (probability) of jumps can be estimated with Kramers' theory [6] as $r_l \propto \exp(-\Delta_l/D)$ and $r_r \propto \exp(-\Delta_r/D)$, where D is the intensity of noise $\xi(t)$. It therefore follows that rates decrease exponentially with increasing B. Consequently even modest increases in B can result in significant reductions in phase diffusion. This is one of the fundamental principles behind the use of IL as a noise mitigation technique. Removal of phase jumps stabilises the frequency and reduces the noise floor. This is clearly shown by the power spectrum of the system Fig. 1(d) where, for $B = 0.5$, IL is observed to sharpen the main spectral line and reduce the broadband noise floor.

Magnetometers

The first use of IL in a magnetometer was reported in a superconducting DC SQUID [7] and then more recently applied to a novel coupled-core fluxgate magnetometer (CCFG) [8]. We review these two systems and also propose a new magnetometer based on a circuit originally proposed by Takeuchi and Harada [9].

Each system is governed by a different set of nonlinear equations and hence the manifestation of IL can be quite different between magnetometers. A comparison reveals a rich spectrum of behaviours that reflects the dynamical complexity of these systems - a complexity that we still do not fully understand.

Although the VdP model serves as a useful paradigm for understanding the dynamics of injection-locked magnetometers, it does not capture all the behaviours observed. The dynamics of a magnetometer strongly depends on the precise nature of the underlying circuit equations. Nevertheless it is possible to make some general statements regarding their operating principles. In particular, once locked the frequency of the oscillations does not depend on the strength of the external target

field. Consequently, field intensity information is only encoded by the amplitude and shape (e.g. duty cycle) of the oscillations; circuits can be design that use either or both mechanisms.

Generally the target magnetic field is a low frequency periodic or aperiodic signal. As a concrete example one could consider the (almost) regular magnetic field oscillations in the Earth's magnetosphere that are typically about 10 nT [10]. These regular fluctuations are called geomagnetic pulsations and appear as nearly sinusoidal waveforms in ground-station magnetometer records with periods ranging from 0.5 s to 10 min [10].

DC SQUID

The DC SQUID is a superconducting loop interrupted by two Josephson junctions, Fig. 2. Its dynamics are described by equations for the Schrödinger phase differences δ_i across the Josephson junctions [7],

$$\tau \frac{d\delta_i}{dt} = \frac{I_b}{2} + (-1)^i I_s - I_0 \sin\delta_i + \xi_i(t), \quad i = 1, 2, \tag{5}$$

where I_s is the circulating current, $I_s = \frac{\Phi_0}{2\pi L}(\delta_1 - \delta_2) - \frac{\Phi_e}{L}$, induced in the loop by an externally applied magnetic flux Φ_e, L is the loop inductance, $\tau = \hbar/(2eR)$ is a characteristic time constant (R being the normal state resistance of the junctions), I_0 is the critical junction current and $\Phi_0 \equiv \hbar/(2e)$ is the flux quantum. The independent additive noise terms $\xi_i(t)$ account for thermal noise arising due to the junction resistances and are modelled as Gaussian and white. The two experimental control parameters are the applied magnetic flux Φ_e and the bias current I_b, which we take to be symmetrically applied to the loop. IL is effected by a periodic modulation of the bias current, $I_b = \hat{I}_b + B\sin(\omega t)$.

This system has been studied experimentally [11], theoretically and by numeric simulation of Eq. (5) [7, 12, 13] with good agreement found between studies. Additionally, excellent progress has been made on the theoretical description of these systems [7]. Nevertheless, there is still much to understand to enable optimised designs to fully take advantage of the IL mechanism.

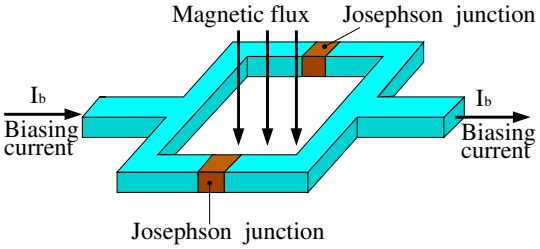

Figure 2: DC SQUID.

Fig. 3 shows the results of numerical simulations in the presence a low frequency target signal. (All numerical simulations were performed for this paper with a custom software written in C that used the Runge-Kutta algorithm of 4-th order adopted to stochastic differential equations [14].) In the unlocked regime (green curve) the signal is manifest as a sharp spectral peak at low frequency superposed on a noise floor background. In the locked case (black curve) the noise floor is suppressed and sidebands appear on both sides of the main locking frequency. The side-

bands, which occur due to a strong heterodyne effect, are amplified versions of the target signal. The amplification gain - defined as the ratio in dB of the sideband amplitude to the low frequency signal amplitude - is shown in Fig. 3b. The large gain, previously reported in [7], suggests signal extraction should occur at the sideband frequencies to reduce the hardware requirements of signal amplification.

It should be noted that the noise floor suppression is also accompanied by a reduction in the amplitude of the target signal and hence the signal-to-noise ratio (SNR) is largely unchanged. Theoretical calculation of the SNR has so far proved intractably and hence it still unknown whether SNR enhancements are possible.

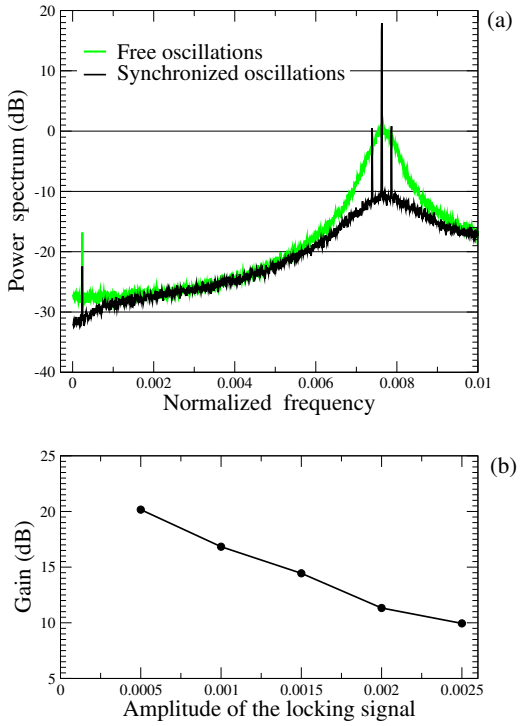

Figure 3: (a) Power spectra of the circulating current in the DC SQUID model Eq. (5). For numerical simulations Eq. (5) was rewritten into a scaled form: $\dot{\delta} = -(2/\beta)(\delta - \pi\Phi_{ex}) - \cos\Sigma\sin\delta$ and $\dot{\Sigma} = J - \cos\delta\sin\Sigma$, where $\delta \equiv (\delta_1 - \delta_2)/2$, $\Sigma \equiv (\delta_1 - \delta_2)/2$, and $J = J_c + A_c + q\sin(\omega t) + A_T\sin(\omega_T t)$, $\Phi_{ex} = \Phi_e/\Phi_0$. Parameters: $J_c = 0.40731$, $A_c = 0.002$, $\omega = 0.0479225$, $q = 0$ for free oscillations (green curve) and 0.001 for locked oscillations (black curve), $\omega_T = 0.03125\omega$, $A_T = 0.00015$, $\beta = 2$, $\Phi_{ex} = 0.495$, $D = 0.000003155$. (b) Dependence of the gain for the left sideband on the amplitude q of the locking signal. The parameters are as in the panel (a).

CCFM

Fluxgate magnetometers represent a broad class of magnetometer that use standard magnetic hysteresis to detect changes in field intensity. They are relatively cheap room temperature devices that can achieve nT accuracy. A number of self-oscillating fluxgate magnetometers have previously been proposed, these include: resonance type oscillators [9, 15], the blocking oscillator [16] and the coupled cores fluxgate magnetometer (CCFM) [17]. This family of oscillators use the target field to modulate the frequency of oscillations or the duty cycle: when the frequency is locked, information about the magnetic field is coded entirely in the duty cycle.

Here we investigate IL in the CCFM. Its basic structure is shown in Fig. 4 and typ-

ically includes three identical modules connected in a ring. The volt-current converter (V-I) injects a current into the primary coil of a fluxgate (FG) and the instrumentation amplifier (INA) picks-up the induced voltage in the secondary coil. This voltage is then integrated to obtain a signal that is proportional to the magnetization of the core in the fluxgate before being amplified (GAIN) and passed to the next module.

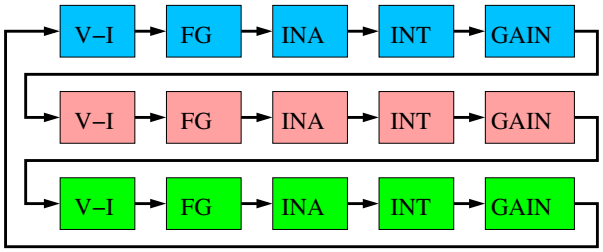

Figure 4: The structure of the CCFM (see text).

Following [17] the model of the CCFM can be written,

$$\begin{aligned}\dot{x}_1 &= -x_1 + \tanh\left[c(x_1 + \lambda x_3 + H_x)\right] + \xi_1(t),\\ \dot{x}_2 &= -x_2 + \tanh\left[c(x_2 + \lambda x_1 + H_x)\right] + \xi_2(t),\\ \dot{x}_3 &= -x_3 + \tanh\left[c(x_3 + \lambda x_2 + H_x)\right] + \xi_3(t),\end{aligned} \tag{6}$$

where x_i is a voltage proportional to the magnetization in the i-th core, c and λ are parameters, $\xi_i(t)$ is a Gaussian white noise with zero mean and noise intensity D. Autonomous (self) oscillations of the CCFM are shown in Fig. 5.

The impact of IL on the CCFM is shown in Fig. 6. Unlike the DC SQUID there is no

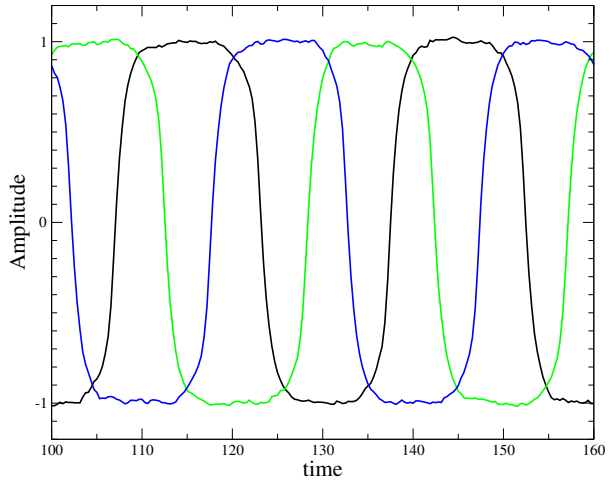

Figure 5: Free oscillations of x_1 (black), x_2 (blue) and x_3 (green) in the CCFM. Parameters are $\lambda = -0.56$, $c = 3$, and the noise intensity is $D = 0.0001$.

signal amplification due to heterodyning but a signal-to-noise ratio (SNR) improvement is observed due to the reduction in the noise floor. This can be quantified by an SNR gain defined as,

$$\Delta_{SNR} = 10\log_{10}\left(\frac{P_1}{N_1}/\frac{P_0}{N_0}\right), \tag{7}$$

where P_0, N_0 are the spectral powers of the signal peak and background respectively in a narrow frequency band centred about the target signal frequency; the subscript zero indicates unlocked oscillations. P_1 and N_1 are the same quantities but for the locked case.

The SNR improvement has previously been reported in experiments and numerical simulations of Eq. (6) [8, 18]. The CCFM has been studied theoretically [17] but, similar to

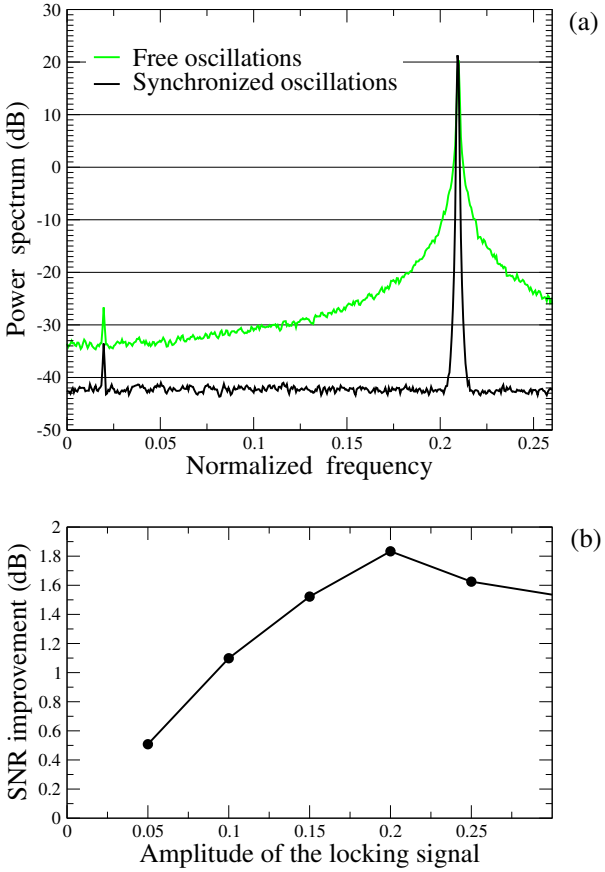

Figure 6: (a) Power spectra for free and locked oscillations in the CCFM. Parameters: $\lambda = -0.56$, $D = 0.0001$; the locking frequency $\omega = 0.628$ is 3 times greater than the natural frequency of the oscillator; the frequency of the target signal is $\omega_T = \omega/32$; the amplitude of the locking and target signal are $q = 0.3$ and $A_T = 0.003$ respectively. The locking signal is added to the target signal $A_T \cos(\omega_T t) + q \cos(\omega t)$. (b) SNR as a function of q.

the DC SQUID, no closed form solution for the SNR exists. The difficulty in obtaining such results limits the ability to optimise system design but equally leaves opportunity for further discoveries and advances to be made.

Modified Takeuchi and Harada magnetometer

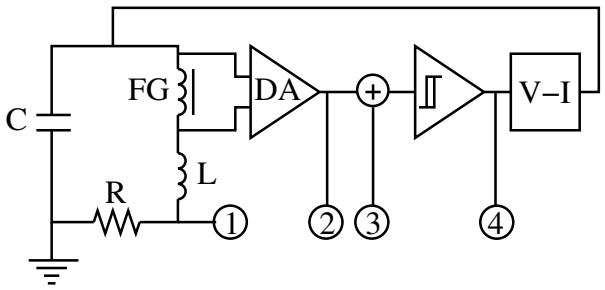

Figure 7: Electric circuit of the magnetometer.

A striking difference between the DC SQUID and CCFM magnetometers is the method of coding used to represent the magnetic intensity information. The heterodyning effect observed in the DC SQUID strongly suggests that information is encoded in the amplitude of the oscillations, in contrast the CCFM is designed to utilise the duty cycle.

To investigate whether SNR improvements can be observed in other duty-cycle based magnetometers we propose a novel system (see Fig. 7) derived from a magnetometer invented by Takeuchi and Harada (TH) [9]. The design has been modified to explicitly utilise the duty cycle and to facilitate theoretical tractability. Another potential practical

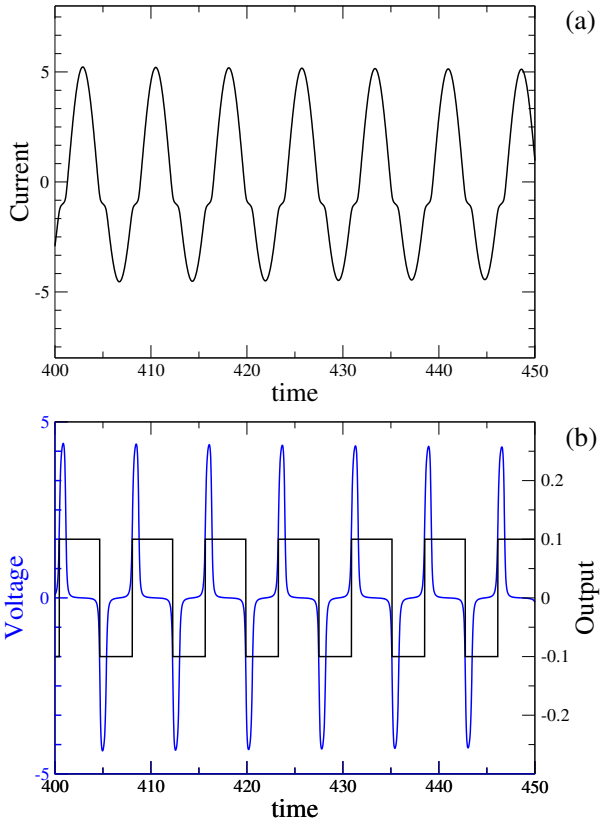

Figure 8: Typical shapes of oscillations. (a) Oscillations of the current I_L in the inductor. (b) Oscillations of voltage in the FG coil and rectangle oscillations of current in the output of the magnetometer. Numerical simulations of Eqs. (8) and (9) were produced for normalized parameters: $k = 10$, $b = 1$, $L = 1$, $R = 0.01$, $C = 1$, $\mu_0 = 1$, $\mu_m = 10$, $S_l = 1$, $l = 1$, $n = 1$, $V_p = 2$.

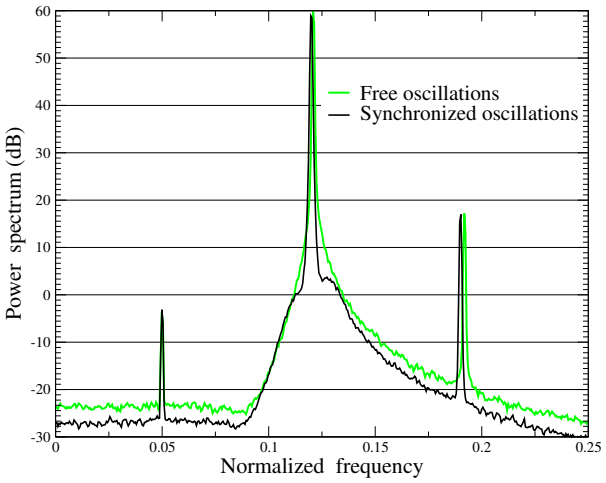

Figure 9: Power spectrum of free and locked oscillations in a presence of a low frequency signal. The power spectrum background is reduced due to the IL. Numerical simulations of Eqs. (8) and (9). Parameters: $k = 10$, $b = 1$, $L = 1$, $R = 0.1$, $C = 1$, $\mu_0 = 1$, $\mu_m = 10$, $S_l = 1$, $l = 1$, $n = 1$, $V_p = 2$.

advantage of this system is its use of resonant amplification to increase the current in the driving coil. This significantly reduces on board power consumption compared to other fluxgate designs; a property that is important for portable measurement systems or when used as a remote sensor node.

In contrast to the original TH circuit, the new design utilises two coils to achieve high Q thus circumventing the need for a large number of turns on the nonlinear core. This improves shielding and simplifies fabrication. Duty cycle coding is achieved through the use of a Schmitt trigger. The mathematical model of this magnetometer is much simpler than the original TH circuit and hence is more amenable to analysis.

The resonance circuit can be described by the following equations for the current I_L in

the inductor (inductance L) and the voltage U_C across the capacitor (capacitance C),

$$\begin{aligned} \dot{I}_L &= (U_C - RI_L)\left(L + n\frac{\partial \Phi}{\partial I_L}\right)^{-1}, \\ \dot{U}_C &= \frac{I_F - I_L}{C}, \end{aligned} \tag{8}$$

where Φ is the magnetic flux in the core of the fluxgate and I_F is the positive feedback current required to induce stable self-oscillation of the circuit. It is assumed that two coils (the inductor and fluxgate) in the circuit are inductive uncoupled (axis are orthogonal). Because the current I_L is proportional to the voltage across the resistor U_R, we can estimate I_L from measurement of U_R at point 1 of the circuit (Fig. 7), i.e. $I_L = U_R/R$. Typical oscillations of the current I_L in the resonance circuit are shown in Fig. 8(a). The voltage in the fluxgate coil can be measured at the output of the differential amplifier (point 2) and is shown in Fig. 8(b).

From Fig. 7 it is observed that the current in the fluxgate coil is identical to I_L therefore we can write,

$$V = n\frac{d\Phi}{dt} = n\frac{\partial \Phi}{\partial I_L}\frac{dI_L}{dt}. \tag{9}$$

Accurate modelling of the magnetic flux Φ is not straightforward, indeed, many models [19] have been proposed. However, if the core is made of a high permeability soft magnetic material with a narrow hysteresis loop, it is possible to use the anhysteretic approximation based on the arctan function

$$\Phi = S_l B(H, I_l) = S_l \frac{\mu_0 \mu_m}{k} \arctan(k(H + bI_L)) \tag{10}$$

where μ_0 is the vacuum permeability, μ_m is a maximum relative permeability of the core material during major hysteresis cycle, and the parameter k is a coefficient of proportionality, H is a target magnetic field; $b = n/l$, n is the number of turns in the coil, l is the length of the coil and S_l is its cross sectional area. Substitution of Eq. (10) and Eq. (8) into Eq. (9) gives an approximation for the voltage in the fluxgate coil,

$$V = n^2 \frac{S_l}{l} \frac{\mu_m \mu_0 (U_C - RI_L)}{L[1 + k^2(H + bI_L)^2] + \mu_m \mu_0}. \tag{11}$$

The voltage V is processed by the differential amplifier and then passed to the Schmitt trigger via the summator where the injection locking signal $s(t)$ is added (point 3). The two thresholds of the Schmitt trigger are chosen such that one is positive V_p and the other negative $V_m = -V_p$. This transforms the intervals between positive and negative pulses into rectangle pulses (point 4 in Fig. 7) from which the duty cycle, and hence field intensity, can be obtained. The rectangular output current is shown in Fig. 8(b).

Given the duty-cycle is proportional to the DC magnetic field H, it follows that the average of the output signal is also proportional to H. This DC current component is fed-back to the coil of the fluxgate and hence results in an additional DC magnetic field that is proportional to H. This positive DC feedback leads to an improved sensitivity of the magnetometer to weak magnetic fields. The DC stability criteria is out of the scope of this paper.

If the magnetic field is not static and H

oscillates with sufficiently low frequency, we may ignore the term dH/dt in the expansion

$$\frac{d\Phi}{dt} = \frac{\partial \Phi}{\partial I_L}\frac{dI_L}{dt} + \frac{\partial \Phi}{\partial H}\frac{dH}{dt} \simeq \frac{\partial \Phi}{\partial I_L}\frac{dI_L}{dt},$$

and use Eqs. (8) and (9) for numerical simulations.

To proceed further the noise sources have to be modelled. These arise from the thermal noise of the resistor, noise in the core of the fluxgate and noise from the Schmitt trigger. We assume the thermal noise is small and hence can be neglected. The noises in the fluxgate core and the Schmitt trigger both impact the precise times of the threshold crossings and hence can be modelled as a common noise applied to the thresholds. This noise gives rise to fluctuations in the frequency of oscillation (when not locked) and the duty cycle. Fluctuations in the LCR circuit are small and hence the period of oscillation of the LCR circuit can be used as a reference for the estimation of the temporal fluctuations.

We now estimate the SNR gain due to injection locking. Let τ_1 and τ_2 be the durations of the positive and negative rectangle pulses respectively. The intervals can then be further decomposed into the following sub-intervals, $\tau_1 = \delta_1 + \Delta_1 - \delta_2$ and $\tau_2 = \delta_2 + \Delta_2 - \delta_3$ where the parameters Δ_1 and Δ_2 are the averaged durations of the positive and negative pulses. We have introduced identically distributed random variables δ_k with variance σ_δ to model the temporal noise (jitter) due to threshold noise. We note that $Z_0(\tau_1 - \tau_2)$ codes the value of the target magnetic field. It is straightforward to find estimates of its mean and variance as $m = Z_0(\Delta_1 - \Delta_2)$ and $\sigma^2 = 6\sigma_\delta^2 Z_0^2$. We now introducing a quantity similar to the SNR, $\eta = m^2/\sigma^2$, that for free oscillations gives $\eta_{free} = (\Delta_1 - \Delta_2)^2/6\sigma_\delta^2$.

The locking signal $s(t)$ should be chosen to suppress noise but preserve the target signal i.e. the locking signal should stabilise the period but not impact the duty cycle. This can be achieved using pulses applied to point 3 in the circuit. An example of such a signal is $s(t) = B\sum_{n=-\infty}^{\infty}\delta(t - nT)$, where T is a period closely related to the frequency of the free oscillations and $\delta(\cdot)$ is the Dirac delta function. In this scenario the temporal jitter associated with one of the thresholds is removed due to the locking. If the period is locked to the positive going oscillation this would yield $\delta_1 = 0$ and $\delta_3 = 0$. Recalculating the mean and variance over a complete cycle yields, $m = Z_0(\Delta_1 - (T - \Delta_1)) = Z_0(2\Delta_1 - T)$ and $\sigma^2 = 4\sigma_\delta^2 Z_0^2$, where it is assumed $\Delta_1 < T < \Delta_1 + \Delta_2$. The reduction in σ^2 for the locked case gives rise to an improvement in the SNR. The SNR gain can be estimated as,

$$\Delta_{SNR} = \frac{\eta_{locked}}{\eta_{free}} = \frac{3}{2}\frac{(2\Delta_1 - T)^2}{(\Delta_1 + \Delta_2)^2} \qquad (12)$$

In the limit $T \to \Delta_1 + \Delta_2$ this approaches $\Delta_{SNR} = 1.5$.

In Fig. 9 spectra for free and locked oscillations are shown. It is observed that the SNR is improved by about 2-3 dB in good agreement with the estimates obtained in this section.

Conclusion

In this paper we have reviewed the IL technique in different magnetometer systems and introduced a novel fluxgate magnetometer circuit. IL impacts magnetometers in different ways depending on the precise detail of the design. The DC SQUID magnetometer showed strong nonlinear mixing (heterodyning) between the locking signal and the natural frequency of oscillation, giving rise to a large amplification of the target signal at the heterodyne frequency. Such effects are expected when the locked oscillations are perturbed in an additive manner by the target magnetic field. In contrast, the two magnetometers that utilised the duty-cycle to code the target signal did not display amplification via heterodyning; rather they showed SNR gains due to the lowering of the spectral background.

It is highly likely that improved designs that utilise amplitude or duty cycle coding (or both) exist. We hope this paper will stimulate research in this direction and encourage further theoretical studies of these systems.

References

[1] Pikovsky, A., Rosenblum, M., and Kurths, J. (2008) Synchronization: Universal Concept: A Universal Concept in Nonlinear Sciences (Cambridge Nonlinear Science Series), Cambridge: Cambridge University Press.

[2] P. S. Landa, Regular and Chaotic Oscillations (Foundations of Engineering Mechanics), Springer (2001)

[3] N.N. Bogoliubov and Y.A. Mitropolsky. Asymptotic methods in the theory of non-linear oscillations, Gordon and Breach Science Publishers 1961. 2. ed.

[4] A. Balanov, N. Janson, D. Postnov, O. Sosnovtseva, Synchronization: From Simple to Complex, 2009, Springer.

[5] R. L. Stratonovich, Topics in the theory of random noise, Vol. 2, Gordon and Breach, New York, 1967.

[6] P. Hanggi, P. Talkner and M. Borkovec, "Reaction-Rate Theory: Fifty Years After Kramers", Review of Modern Physics 62:251-341 April 1990

[7] M. E. Inchiosa, V. In, Adi R. Bulsara, K. Wiesenfeld, T. Heath, M. H. Choi, "Stochastic dynamics in a two-dimensional oscillator near a saddle-node bifurcation", Physical Review E 63, 066114 (2001)

[8] F. Antoci, B. Ando, C. Trigona, A. Kho, A. Nikitin, N. Stocks, A. R. Bulsara and S. Baglio, "Injection Locking in Coupled Core Fluxgate Magnetometers: Exploiting Nonlinearity to Enhance Sensitivity Toward Weak, Low Frequency, Target Magnetic fields", IEEE Sensors Journal 14(2):554-562, 2014

[9] S. Takeuchi and K. Harada, "A Resonant-Type Driven Amorphous Ribbon Magnetometer by an Operational

Amplifier", IEEE Transactions on Magnetics, Vol. MAG-20, No. 5, 1984, 1723-1725

[10] B. J. Anderson, "Ultra-Low-Frequency Magnetic Pulsations in the Earth's Magnetosphere", Johns Hopkin s APL Technical Digest, Vol. 11 , No 3 and 4, 239-254 (1990)

[11] A.R. Bulsara, J.A. Acebron, W.-J. Rappel, A. Hibbs, L. Kunstmanas, M. Krupka, "Injection locking near a stochastic bifurcation: the dc SQUID as a case study", Physica A 325 (2003) 220 - 229

[12] K. Wiesenfield, A. R. Bulsara and M. E. Inchiosa, "Oscillatory dynamics of a nonlinear amplifier in the high-gain regime: Exploiting a global connection", Physical Review B 62, No 14 (2000) R9232

[13] A. Palacios, J. Aven, P. Longhini, V. In, and A. R. Bulsara, "Cooperative dynamics in coupled noisy dynamical systems near a critical point: The dc superconducting quantum interference device as a case study", Physical Review E 74, 021122 (2006)

[14] V. Mackevicius, Introduction to Stochastic Analysis: Integrals and Differencial Equations, ISTE, London, 2011.

[15] M. Z. Kozak, E. Misiuk, and W. Kwiatkowski, "A convertertype magnetometer using amorphous ribbon or wire" Journal of Applied Physics 69, 5023 (1991); doi: 10.1063/1.348162

[16] Robert E. Brown, "Oscillator/Driver Circuit for Fluxgate Magnetometer", United States Patent 4,384,254, May 17, 1983

[17] Visarath In, Antonio Palacios, "Coupled-Core Fluxgate Magnetometer" in "Symmetry in Complex Network Systems: Connecting Equivariant Bifurcation Theory with Engineering Applications" Chapter 2, Springer 2018

[18] B. Ando, S. Baglio, C. Trigona, A.R. Bulsara, N.G. Stocks, A. Nikitin, "Injection-Locking Benefits for weak AC magnetic field detection in Coupled-Core Fluxgate Magnetometers", 2012 IEEE International Instrumentation and Measurement Technology Conference Proceedings. Article number 6229707, 318-322. DOI: 10.1109/I2MTC.2012.6229707

[19] W. A. Manly, "An Appraisal of Several Nonlinear Hysteresis Loop Models", IEEE Transactions on Magnetics, Vol. MAG-9, No 3, 1973, 256-260

Alexander Nikitin received the Ph.D. degree in physics and mathematics from the Saratov State University, Russia, in 1999. He currently is a Research Fellow at the University of Warwick, U.K. His research interest includes the biophysics and the information theory, nonlinear systems in the presence of

noise, microscopic sensors and complex sensory systems.

Nigel G. Stocks is currently Director of the Warwick Centre for Predictive Modelling at the University of Warwick. He received a First Class B.Sc. degree in applied physics and electronics from Lancaster University in 1987 and the Ph.D. degree in stochastic nonlinear dynamics in 1991. His early research was in the area of information processing in noisy systems and specifically stochastic resonance and suprathreshold stochastic; more recently he has developed interests in neural and biological signal processing, biomimetic engineered systems and cochlear implant coding.